Chapter 14

An Ultracompact Real-Time Fluorescence Loop-Mediated Isothermal Amplification (LAMP) Analyzer

Gihoon Choi and Weihua Guan

Abstract

Low-cost access to the highly sensitive and specific detection of the pathogen in the field is a crucial attribute for the next generation point-of-care (POC) platforms. In this work, we developed a real-time fluorescence nucleic acid testing device with automated and scalable sample preparation capability for field malaria diagnosis. The palm-sized battery-powered analyzer equipped with a disposable microfluidic reagent compact disc described in the companion Chap. 16 which facilitates four isothermal nucleic acid tests in parallel from raw blood samples to answer. The platform has a user-friendly interface such as touchscreen LCD and smartphone data connectivity for on-site and remote healthcare delivery, respectively. The chapter mainly focuses on describing integration procedures of the real-time fluorescence LAMP analyzer and the validation of its subsystems. The device cost is significantly reduced compared to the commercial benchtop real-time machine and other existing POC platforms. As a platform technology, self-sustainable, portable, low-cost, and easy-to-use analyzer design should create a new paradigm of molecular diagnosis toward a variety of infectious diseases at the point of need.

Key words Point-of-care, Nucleic acid testing, Real-time, Fluorescence, Analyzer, Malaria

1 Introduction

In the current healthcare landscape, the ability to diagnose, monitor, and manage diseases near the site of patient care is increasingly essential for rapid clinical decision-making [1, 2]. Over the past decade, point-of-care (POC) technologies have been offered accessible diagnosis, low-cost, reduced sample/reagent volumes, and rapid analysis time. Current POC devices for pathogen screening in the field almost exclusively focus on immunoassay-based rapid diagnostic tests (RDTs), which can detect various biological analytes (e.g., cholesterol, lipids, HbA1c, cardiac markers, CD4+, HIV proteins, histidine-rich protein II, influenza, cardiac marker, and cancer markers) [2]. The integrated colorimetric and fluorometric lateral flow assay in paper strips [3] and microfluidic reagent cartridge [4] were analyzed by electrochemical and optical readout

Miguel R. Ossandon et al. (eds.), *Biomedical Engineering Technologies: Volume 1*, Methods in Molecular Biology, vol. 2393, https://doi.org/10.1007/978-1-0716-1803-5_14, © Springer Science+Business Media, LLC, part of Springer Nature 2022

using smartphone methods, allowing excellent portability, simplicity, low-cost, and fast turnaround time. However, most RDTs have an insufficient limit of detection to identify samples with low analyte concentration [5]. The insufficient detection limit is often problematic for the identification of asymptomatic carriers in the case of infectious diseases (e.g., malaria parasite, HIV, HPV, Zika, Ebola, and dengue) where early diagnosis and timely treatment is essential to prevent the transmission of diseases [6].

Nucleic acid testing (NAT) methods enable much-enhanced sensitivity [7, 8], which is highly desired for identifying asymptomatic infections [7, 9–12]. Among various molecular amplification assays, loop-mediated isothermal DNA amplification (LAMP) has emerged as a promising technology for field use due to its simplicity, rapidness, sensitivity, and specificity [8, 9, 11, 13–15]. In particular, LAMP has been used in POC application due to its robustness against the crude samples (blood, saliva, nasal swab, etc.), which contains amplification inhibitors [16–18]. Unfortunately, most LAMP-based test still requires bulky peripheral equipment and skilled technicians for the sample process [8–22]. Besides, necessary infrastructures such as electricity for powering equipment are often limited in remote clinical settings [23–25]. Therefore, there is a strong desire to develop a molecular diagnostic system that can be easily deployed to clinical sites.

Various POC LAMP platforms were reported to enable highly sensitive field diagnosis. For example, electric-free noninstrumented nucleic acid amplification (NINA) platform uses exothermic chemical reaction as a heating element to facilitate colorimetric RT-LAMP assay for a qualitative HIV-1 and malaria test in a tube [26, 27]. Microfluidic Biomolecular Amplification Reader (μBAR) system was developed by converging microfluidics, optics, and electronic technologies to perform NATs on microfluidic reagent cartridge for quantitative HIV-1 testing [20]. A battery-powered compact genetic testing instrument (Gene-Z) were integrated with multi-channel fluorescence sensors and aluminum heater for multiplexed detection for foodborne pathogens such as *E. coli* and *S. aureus* [28]. Many CD-like centrifugal platforms [29] for the LAMP test were also reported to achieve high-throughput and multiplexed detection of foodborne pathogens [30].

Despite significant effort and progress toward field deployment of NATs assays, highly integrated DNA sample preparation from raw peripheral blood for molecular assays remains a bottleneck [31, 32]. Current sample preparation usually involves lengthy or error-prone manual processes such as gravity-driven filtration [33], centrifugation [34]. Although a few emerging POC NAT devices (e.g., Alere q system [35, 36], Cobas Liat system [37], and Cepheid Xpert Omni platform [38]) have successfully integrated the sample preparation step, a low-cost LAMP-based NAT is not readily available for the screening test. For the promising LAMP technologies

to be used as malaria screening tests in the field, the DNA extraction method should be simple, rapid, scalable, fully automated, free of cross-contamination, and seamlessly integrated with the amplification for immediate analysis.

POC technologies play an important role in modern healthcare industries since they can expedite the flow of patient care, reduce the wait times and cost, and increase the access to sensitive and specific diagnostics. The ASSURED (Affordable, Sensitive, Specific, User-friendly) criteria are the key considerations for POC device development. Recent POC technologies focus on mobile and automated platforms that open up the diagnostic opportunities in a resource-limited setting where the well-established healthcare infrastructures and quality medical care are not available. Besides, simplicity and ease of use are attributes of most POC devices, allowing patients to perform self-testing (e.g., glucose, HIV, STD, and malaria) at the primary care before seeing healthcare professionals.

A microcontroller is a miniaturized computer on a single integrated circuit. A typical MCU includes a processor, memory, and input/output peripherals. MCU also supports analog-to-digital converter (ADC), and digital-to-analog converter (DAC) allows the microprocessor to interface with external analog sensor devices without additional computing components. Due to its small size, low-power consumption, and cost, it has been widely used in portable electronic devices such as cellphones, cameras, and medical devices. Those attributes can be applied to the POC LAMP devices, which often requires an automatic process for controlling peripheral electronics such as digital image sensor, thermal module, display, and data interfacing module.

Here, we present a real-time fluorescence LAMP device suitable for field detection of malaria with automated and scalable sample preparation capability (Table 1). The palm-sized platform unprecedentedly integrated with thermal, optical, electromechanical, data/interfacing subsystems for streamlined nucleic acid sample process from raw blood samples to isothermal amplification preformed in a disposable microfluidic reagent compact disc described in the companion Chap. 16. More specifically, a restive heating source was feed-back controlled to maintain the isothermal nucleic acid amplification temperature at 65 °C. The optical module consists of an optical excitation source and color sensors, enabling the detection of green fluorescence light during the nucleic acid amplification process. The servo motor was used to rotate the microfluidic reagent compact disc against the stationary permanent magnet to actuate the magnetic beads to the designated reagent chambers on the disc for performing magnetic interaction–based nucleic acid sample extraction/purification assay. Touchscreen display provides a user-friendly interface for ease of use. During the amplification process, the optical signal was real-time

Table 1
Comparison of NAT POC devices for malaria diagnosis. (Reproduced from Biosensors and Bioelectronics 2018 with permission from Elsevier [48])

Assay	Detection method	Real-time ability	Automation	Sample processing	LOD (p/μl)	"Sample-to-Answer" Turnaround Time	References
LAMP	Fluorescence	Yes	Automated	Magnetic bead-based extraction	0.6	<40 min	This work
LAMP	Turbidity	No	Manual	Gravity-driven filtration	2	<1 h	[33]
LAMP	Turbidity	No	Manual	Thermal lysis centrifugation	5	60–80 min	[34]
LAMP	Fluorescence	Yes	Manual	Gravity-driven filtration	5	45 min	[42]
LAMP	Hydroxynaphthol blue (HNB)	No	Manual	Saponin–Chelex lysis	1–5	Not reported	[43]
PCR	Fluorescence	Yes	Manual	Off-chip	5	<1 h	[44]
PCR	Fluorescence	Yes	Manual	Off-Chip	2	Not reported	[45]
RPA	Interferometer	Yes	Manual	Dimethyl adipimidate/ thin film extraction	1	~1.2 h	[46, 47]
HDA	Lateral flow strip	No	None	None	200	~2.5 h	[48]

plotted on the embedded screen or smartphone via an integrated Bluetooth module. The user can perform post-analysis since raw data were stored in the memory card through a micro SD card module. The detailed automated sample process on microfluidic reagent compact disc will be discussed in the Chap. 16. The platform is capable of processing four samples simultaneously in parallel. The device dramatically minimizes the manual workload needed for performing the NATs and offers low-cost and accurate diagnosis performance quickly and automatically at point of need.

2 Materials

2.1 Instrumentation

1. Materials and supplies: Table 2

   Thermal Subsystem: Aluminum plate (CP-0.91-0.91, custom Thermoelectric), power resistor (PWR263S-20-2R00J, Digi-Key), N-channel power MOSFET (63J7707, Digi-Key), thermistor (95C0606, Digi-Key), epoxy (DP100-clear, 3M), thermal paste (AATA-5G, Artic Alumina).

Table 2
Bill of materials for the analyzer. (Reproduced from Biosensors and Bioelectronics 2018 with permission from Elsevier [48])

System	Description	Part#	Function	Unit cost ($)	Unit Qty.	Ext. cost ($)
Electronics	Arduino Mega 2560 R3	DEV-1106	Microcontroller	45.95	1	45.95
Electronics	36-pin stripe male header	392	Headpins	4.95	0.083	0.41
Electronics	DC barrel power Jack/ connector	PRT-00119	Power connector	1.25	1	1.25
Electronics	Shield stacking headers for Arduino	85	Wire sockets	1.95	0.33	0.64
Electronics	Premium male/male jumper wires	758	Wires	3.95	0.75	2.96
Electronics	Trimmer potentiometer, 500 Ω	62J1468	LED adjustment	1.98	4	7.92
Electronics	Through hole resistor, 10 kΩ	38K0328	Temperature control	0.09	5	0.45
Electronics	Through hole resistor, 47 Ω	38K0326	Resistors for LED	0.09	2	0.18
Electronics	Capacitor 470 μF	65R3137	Power stabilizing	0.11	1	0.11
Electronics	Capacitor 0.33 μF	46P6304	Voltage regulating	0.27	1	0.27
Electronics	Capacitor 0.1 μF	46P6667	Voltage regulating	0.354	1	0.354
Electronics	Diode, standard, 1 A, 50 V	78K2043	Diode	0.07	1	0.07
Electronics	26 pin wire connector	1171	Wiring	4.95	1	4.95
Electronics	26 pin GPIO ribbon cable	862	Wiring	2.95	1	2.95
Servo	Micro size - high torque servo	2307	Actuation of disc	11.95	1	11.95
Magnets	Neodymium disc magnet nickel	58605K33	Holding magnetic beads	2.69	4	10.76
Thermal	Cold plate	CP-0.91-0.91	Heating stage	5.75	0.25	1.44
Thermal	Power resistor	PWR263S-20-2R00J	Heater	4.12	4	16.48
Thermal	N Channel power MOSFET	63J7707	Switch for Peltier heater	1.66	1	1.66
Thermal	Thermistor	95C0606	Temperature sensing	7.34	1	7.34
Optics	Color sensor	1334	Detection	7.16	4	28.64

(continued)

Table 2
(continued)

System	Description	Part#	Function	Unit cost ($)	Unit Qty.	Ext. cost ($)
Optics	Optical plastic light guide	#02-538	Guiding light	2.55	0.24	0.61
Optics	CREE LED, blue, T-1 3/4 (5 mm)	04R6674	Fluorescence excitation	0.21	1	0.21
Bluetooth	Bluetooth low energy (BLE 4.0)	1697	Bluetooth connectivity	19.95	1	19.95
LCD	3.5″ TFT 320 × 480	85	Touchscreen LCD	39.95	1	39.95
SD	MicroSD card breakout board	254	SD module	7.5	1	7.50
Enclosure	Adjustable-friction hinge	1791A44	Hinge	6.72	2	13.44
Enclosure	ABS filament	90003001	3D platform material	18.5	0.4	7.40
Enclosure	Acrylic sheet, 1/8″ thick, 12″ × 24″	8505K12	Holding plates	13.46	0.7	9.42
Enclosure	Screws (M4 cap screw)	W8S038	Hinge holding	3.25	0.04	0.13
Enclosure	Screws (M3 set screw)	SS3M6	For holding color sensor	9.25	0.0006	0.01
			Total cost			**$245.35**

Optical subsystem: Color sensor module (1334, Adafruit), Optical grade plastic light guide (dia. 2.8 mm, #02-538, Edmund Optics), Optical grade plastic light guide (dia. 1 mm, #02-536, Edmund Optics), Blue LED (04R6674, Digi-Key).

Electromechanical subsystems: Capacitor 470 μF (65R3137, Digi-key), High torque servo motor (2307, Adafruit), Neodymium disc magnet (58605K33, McMaster), 5 V voltage regulator (L7805CV, Digi-Key), Acrylic solvent (IPS4-4OZ, ePlastics), and 1/8″ acrylic sheet (8505K12, ePlastics).

Data/Interfacing subsystem: microSD card breakout board (254, Adafruit), 3.5″ TFT Touchscreen breakout (2050, Adafruit), BLE 4.0 breakout (1697, Adafruit).

2. 3D printer (MakerBot Replicator+, USA).
3. CO_2 laser cutting machine (Epilog Helix 24 Laser System, USA).
4. Custom printed circuit boards (PCB) were manufactured by the commercial vendors (OSH Park, USA).

5. CAD software: Eagle PCB design tool (Autodesk, USA), AutoCAD (Autodesk, USA), and SolidWorks 2015 (DS SolidWorks Corp., USA).
6. MCU programming: Arduino software (IDE).

3 Methods

The real-time LAMP Analyzer presented here designed to amplify DNA in a disposable microfluidic compact disc described in the companion Chap. 16.

3.1 Analyzer Overview

1. The assembled and exploded views of the analyzer are shown in Fig. 1.
2. The analyzer has four parallel testing units and has a small footprint of $10 \times 12 \times 12$ cm^3.
3. The fully integrated analyzer consists of thermal, optical, electromechanical, and data/interfacing subsystems. The functional subsystems inside the analyzer are illustrated in the block diagram (Fig. 2).
4. A customized printed circuit board (PCB) with an embedded microcontroller unit (MCU) operates the whole device from sample preparation to result (Fig. 2).
5. A rechargeable 9 V portable Lithium-ion battery powers the entire system and could last for >15 h before recharging (Fig. 2).

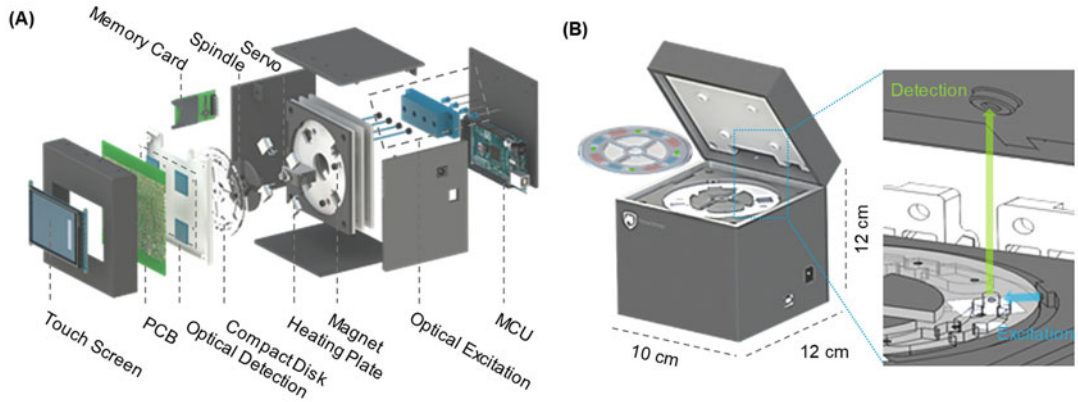

Fig. 1 Overview of the device. (**a**) Exploded view of the device, showing the assembly of various components. (**b**) Schematic of the assembled device and the quadplex microfluidic reagent compact disc. The form factor of the analyzer is palm-sized. The reagent compact disc is secured to the spindle platter. A real-time fluorescence sensing scheme is integrated on the analyzer. (Reproduced from Biosensors and Bioelectronics 2018 with permission from Elsevier [40])

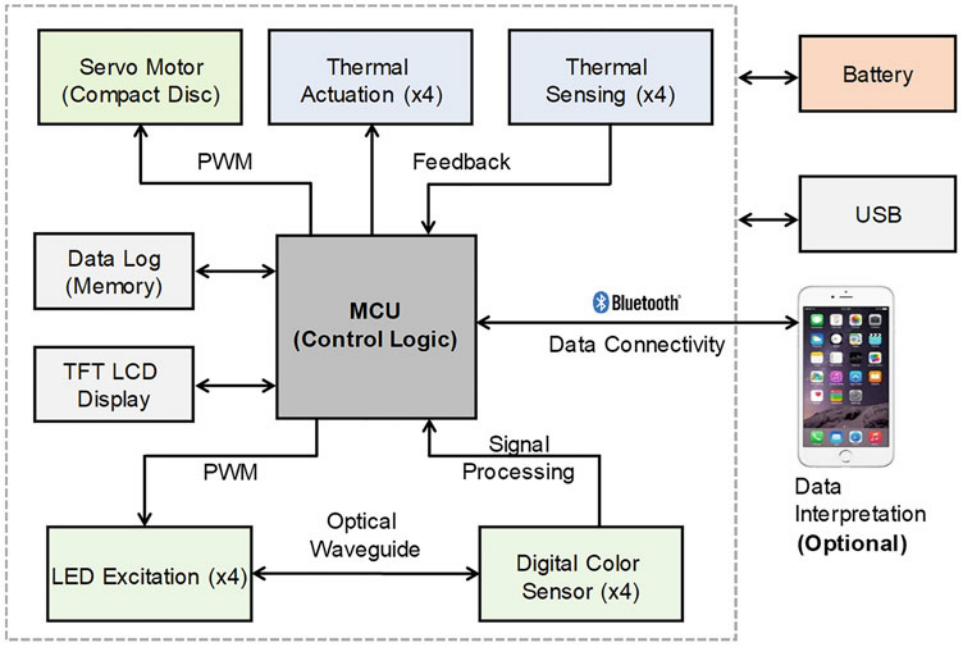

Fig. 2 System block diagram with interconnected subsystems. The platform consists of four main functional subsystems: mechanical subsystem (servo motor/spindle platter/compact disc), an optical subsystem (LED/optical sensor), a thermal subsystem (heater/thermal sensor), and data subsystem (Bluetooth). Each module was controlled by a microprocessor on a customized PCB board. The diagnostic results can be optionally reported to a smartphone user interface. (Reproduced from Lab on a Chip 2016 with permission from the Royal Society of Chemistry [41])

3.2 Thermal Subsystem

1. The thermal module consists of four resistive-heating elements (2 Ω power resistor for each), N-channel power MOSFET, and microthermistor. Figure 3a shows one unit of the thermal module. The 9 V rechargeable battery (max output current: 2 A) was used to power the heating elements via control PCB, which contains control circuits for all subsystems (Fig. 4a).
2. *Fabrication steps:* Four resistive-heating elements were connected in series with wires to maintain the uniform temperature among each testing unit (Fig. 3b, c). The aluminum heating plate was drilled from the side to make space for micro-thermistor, which were embedded in the center of the heating plate for real-time temperature monitoring (Fig. 3b). After inserting the thermistor, we introduced a drop of epoxy to fix it. Each power resistor was bonded to the backside of an aluminum heating plate by thermal paste.
3. To simplify the wiring, most electronic circuits for the thermal module were integrated into the control PCB (Fig. 4a). Only active components such as heating elements and thermistors were wired using jump wire to place them close to the reaction

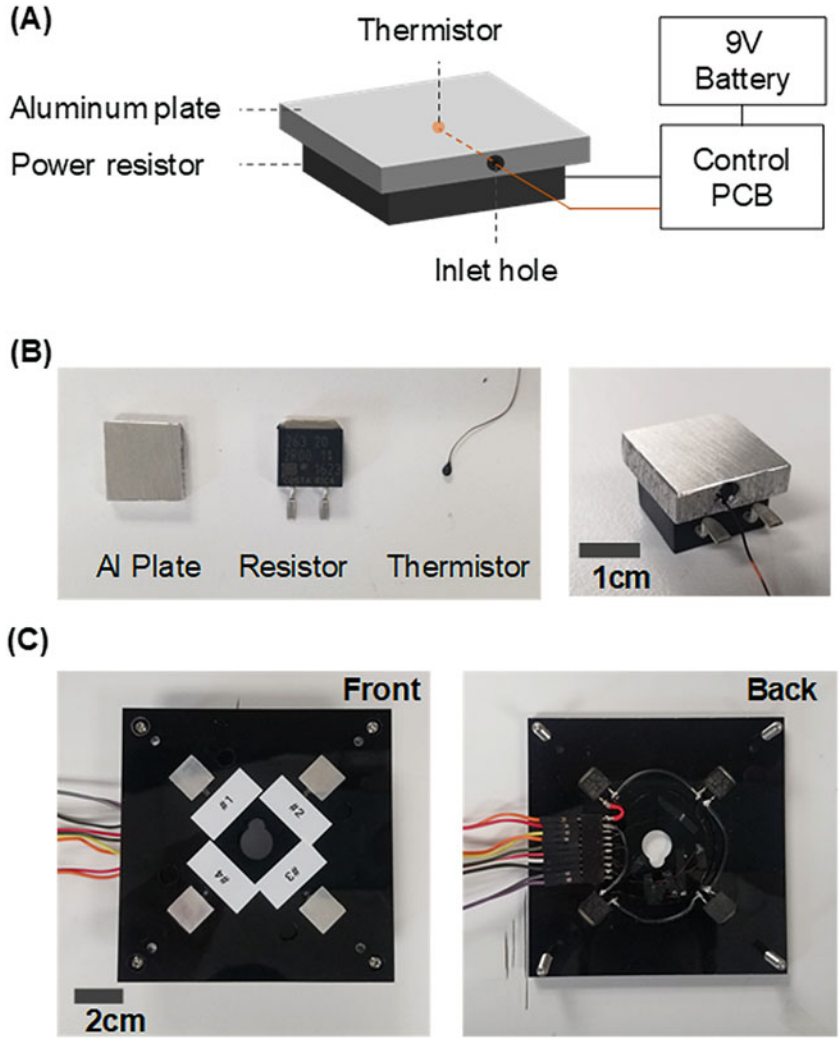

Fig. 3 Integrated thermal subsystem. (**a**) Schematic of the thermal subsystem. The thermistor is embedded in the Aluminum plate. Control PCB interfaces with a thermistor to monitor temperature and supply the power to the resistive heating element. (**b**) Photo image of each component and assembled thermal unit. (**c**) 4-plex thermal module integrated into the analyzer part. Four heating elements were connected in series using wires

chamber on a reagent compact disc. Figure 4b showed a detailed thermal control circuit diagram.

4. Negative feedback control was used to maintain the desired constant temperature (65 °C) during the DNA amplification (Fig. 5). The N-channel power MOSFET was controlled using digital output from MCU. For example, MOSFET shuts off when temperature reading overshot the set temperature. Whereas, the MOSFET was turned on when the temperature reading was lower than the set temperature.

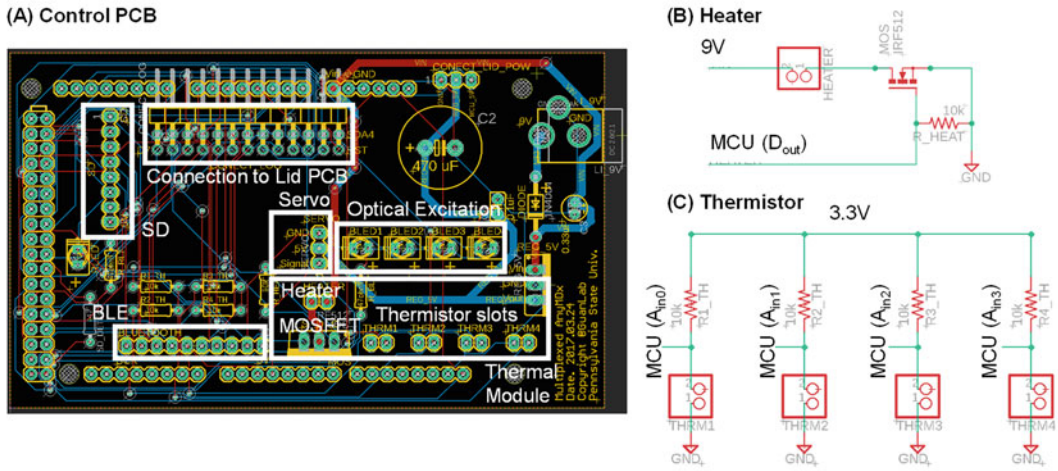

Fig. 4 Electronics for the thermal subsystem. (**a**) Control PCB design. The thermal module is integrated into the control PCB. The actual heating element and thermistors were connected to the pin connector on the PCB board using wires. (**b**) Circuit diagram for heating element control. A 9 V external battery powers the heating sources. The digital output from MCU gates the MOSFET. (**c**) Circuit diagram for the thermistor circuit to measure the temperature. 3.3 V was used as a reference voltage to obtain the resistance of the thermistor based on its temperature

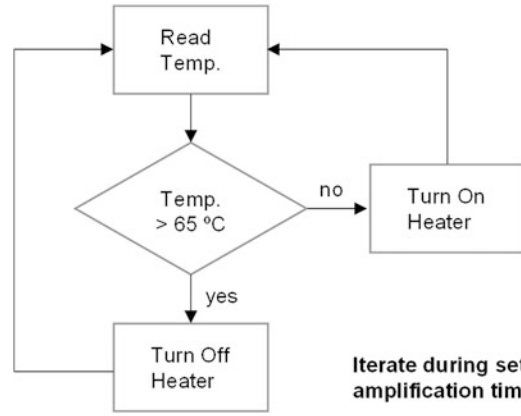

Fig. 5 Feedback thermal control sequence. The most recent temperature from the thermistor is compared with the set temperature (65 °C). If the current temperature is higher than the set temperature, the heater is electronically shut down by the MOSFET switch. If the current temperature reading is lower than the set temperature, the heater is turned on. This process repeats until the amplification process ends

5. A custom-built thermal control code was uploaded into the MCU board through the computer using open-source Arduino Software (IDE). The program reads and updates the most recent temperature values every 3 s during the DNA amplification process. The temperature reading was recorded on a micro

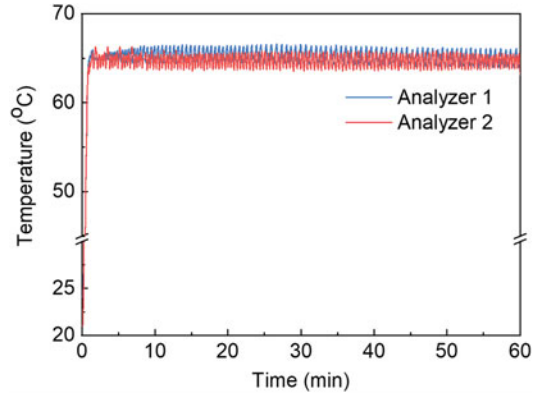

Fig. 6 The feedback-controlled reaction temperature profiles as a function of time (blue curve: Analyzer 1, red curve: Analyzer 2). (Reproduced from Lab on a Chip 2016 with permission from the Royal Society of Chemistry [41])

SD card for validation purposes. Once the code is uploaded, MCU can operate the thermal control sequence by itself without a computer connection.

6. To evaluate the temperature fluctuation, the temperature was monitored for 60 min by an external independent thermocouple module (NI-9211, National Instruments).
7. Figure 6 shows the temperature on the aluminum heating plate can reach the set temperature (65 °C) within 40 s and continuously maintain a temperature between 64.5 and 66.5 °C.

3.3 Optical Subsystem

The microfluidics assay presented in this chapter is performed with an automated device described in the companion Chap. 16.

The automated device described in the companion Chap. 16.

1. For real-time tracking of fluorescence signal during the DNA amplification, we used a blue LED ($\lambda = 488$ nm) as an optical excitation light source and color sensor as an optical detector (Fig. 7). Four blue LEDs were embedded in custom-built fiber coupler and directed toward individual reaction chambers through polymer optical fibers (*see* **Note 1** for fiber preparation). The incidence of the excitation light was perpendicular to the optical sensor to minimize the excitation interference (Fig. 7). The green cellophane film was used only to allow the green light to the color sensor.
2. Customized fiber coupler was 3D printed to facilitate the tight coupling of an incoherent LED light source to the optical fiber (Fig. 8a). On the bottom side of the fiber coupler, there are four spatially isolated LED holes to mechanically secure the LED blubs and vertically align with the optical fiber. Similarly, front of the optical fiber was inserted from the top side of the coupler and mechanically secured by the epoxy. Optical fiber

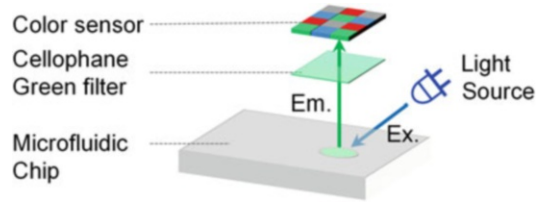

Fig. 7 Schematics for fluorescence sensing module. The blue LED ($\lambda = 488$ nm) excites fluorescence dye from the side of the microfluidic chip. The color sensor is vertically aligned with the reaction chamber and monitors the green emission light ($\lambda = 515$ nm) from the microfluidic chip (*see* also Fig. 1b). The green cellophane film was placed below the color sensor to minimize the background by filtering red and blue light

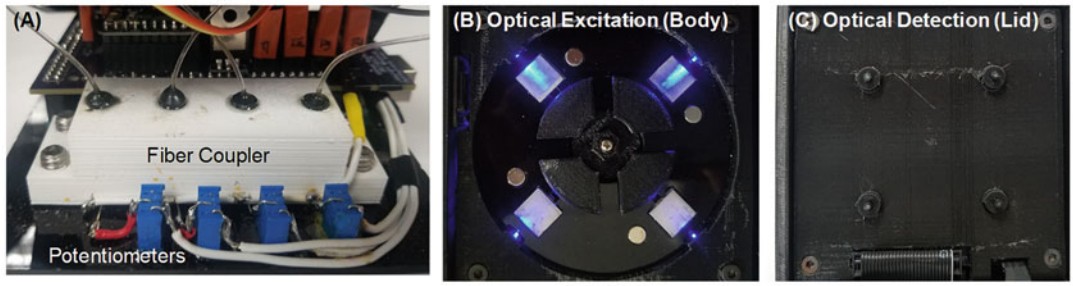

Fig. 8 Photo image of the integrated optical subsystem. (**a**) Custom-built fiber coupler. The blue LED light sources were inside of the fiber coupler. The plastic optical fiber socket was aligned with the center of the blue LED bulb top. Potentiometers were connected with each blue LED to calibrate the intensity manually. (**b**) Optical excitation. The output of blue LED lights shines from the 3D printed sidewalls. (**c**) Optical detection. The image showed the lid side of the analyzer. The color sensors were embedded inside the analyzer lid. The locations of the four optical fibers were where the four-color sensors were placed

end was inserted into the 3D printed fiber holder and fixed by epoxy (*see* Fig. 8b). The optical detection side fibers were secured on the 3D printed lid cover (*see* Fig. 8c). When the lid was closed, the optical fibers aligned with the reaction chamber in the microfluidic chip. Black enclosure covers entire optical subsystem components (e.g., fibers, LEDs, and color sensors) to prevent interference from unwanted background light.

3. The color sensor (TCS3472, TAOS) includes a 3×4 photodiode array, four Analog-to-Digital Converters (ADC), data registers, and I^2C interface. The photodiode array comprises red-filtered, blue-filtered, and green-filtered photodiodes; thus, it is capable of RGB sensing (Fig. 7). The four ADCs convert the amplified photodiode current to 16-bit digital output in parallel. The digital outputs were sent to the MCU through the I^2C communication port at 400 kHz. Internal integration time and gain can be adjusted by accessing the

register setting. The TCS 3472 has a timing register that can control the internal integration time of ADC channels (2.4, 24, 50, 101, 154, 700 ms). Similarly, internally generated gain (1×, 4×, 16×, and 60×) can be selected for conversion by accessing the control register. The longer integration time and higher gain increase sensitivity at the low light level. For the optimal green fluorescence detection, we set the gain at 60 and integration time at 700 ms. Note that gain and integration time should be carefully determined based on the experimental and environmental conditions due to the dynamic range of the color sensor (*see* **Note 2**). Dark ADC count has a range of 0 to 5, which is differ by two to three orders of magnitude with green fluorescence light count (Fig. 10a). The color sensor was designed to operate in the temperature range of −30 to 70 °C. We operated the sensor at uniform room temperature (25 °C), and no temperature-dependent noise, such as thermionic emission, was observed.

4. Figure 9 shows the circuit diagram of the optical module. Each LED was connected in parallel to ensure the uniformity of the excitation light (Fig. 9a). Potentiometers were used to calibrate the optical uniformity further (*see* **Note 3**). Figure 9b shows schematics for the optical detection sensor wiring. The sensor was powered by Arduino (3.3 V). The I^2C bus (SCL and SDA) was connected to the MCU for data transfer. The received optical data was recorded in a micro SD card via the integrated SD card breakout.

5. *Uniformity.* For the quadruplex parallel NAT device, the fluorescence sensing consistency among different channels is essential for quantitative analysis. We tested fluorescent Calcein dye at various known concentrations. At each concentration, identical Calcein aliquots were loaded into the four reaction chambers for fluorescence intensity measurement. Figure 10a shows the relative fluorescence unit (RFU) distribution from each optical channel at different concentrations. The quantitative uniformity among the four channels is excellent, as seen by the small standard deviation for the RFU values. Moreover, as expected, the mean fluorescence intensity was proportional to the Calcein concentration, and a twofold Calcein concentration difference could be discriminated (inset in Fig. 10a). To further validate the fluorescence sensing uniformity during the real-time LAMP process, four identical 1 μl of *Pf* genomic DNA was directly loaded into each reaction chamber, and the real-time amplification curve was monitored (Fig. 10b). We repeated each test three times. The variation of threshold time (T_t) among different fluorescence sensing channels was ~1.5 min (inset of Fig. 10b). These results validate the fluorescence sensing uniformity among different optical channels.

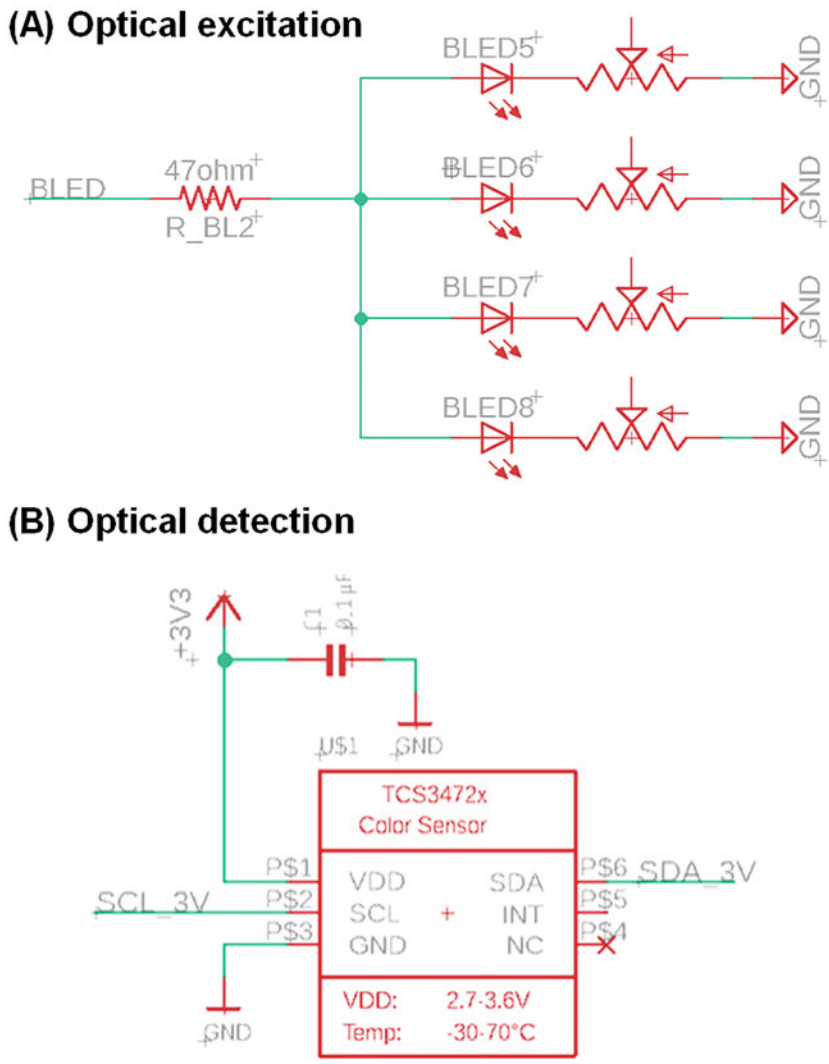

Fig. 9 Circuit diagram for the optical module. (**a**) Optical excitation circuit. (**b**) Optical detection circuit. 3.3 V was derived from the MCU to power the color sensors. SCL and SDA pins were wired to the MCU for I^2C communication

6. *Quantitative*. A series of tenfold dilutions of *Pf* genomic DNA in Tris-EDTA buffer was used to validate the quantitative ability of the device. For each concentration, a set of three identical *Pf* genomic DNA samples and one internal negative control were loaded into each of the four reaction chambers on the disc. The DNA sample volume is 1 µl, and the LAMP master mix is 24 µl. Figure 10c shows real-time amplification results from various concentrations of *Pf* genomic DNA. The mean and standard deviation of the amplification threshold time (T_t) was obtained from the triplicates for each concentration. As shown in the bottom subplot of Fig. 10c, a clear linear

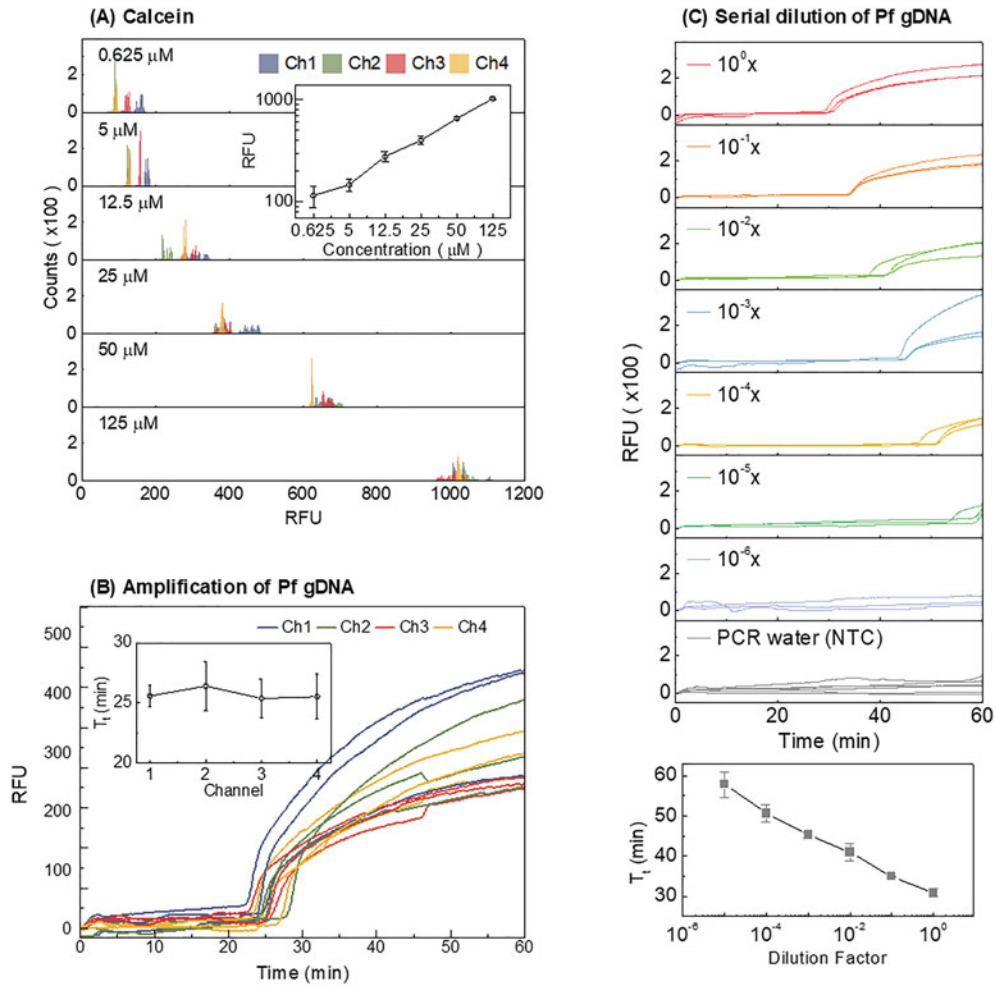

Fig. 10 Validation of the optical sensing uniformity. (**a**) With fluorescent Calcein dye, the RFU distribution for the four optical channels was evaluated at a series of Calcein concentration. A linear dependence of the RFU on the Calcein concentration was observed in the range of 0.625–125 μM. The RFU variation from the four channels is small. (**b**) With *Pf* genomic DNA at constant concertation, the variations of the amplification threshold time (T_t) obtained from the real-time curve is ~1.5 min. (**c**) Amplification curves for tenfold serially diluted *Pf* genomic DNA samples. The bottom plot shows the calibration curve for the *Pf* genomic DNA. Standard deviation values are from triplicates. (Reproduced from Biosensors and Bioelectronics 2018 with permission from Elsevier [40])

relationship was observed between T_t and the dilution factor, which could be used as a reference curve for quantification. The quantitative ability is important for assessing parasite load in the blood, a useful indicator for determining the proper anti-malarial drug dosage [39].

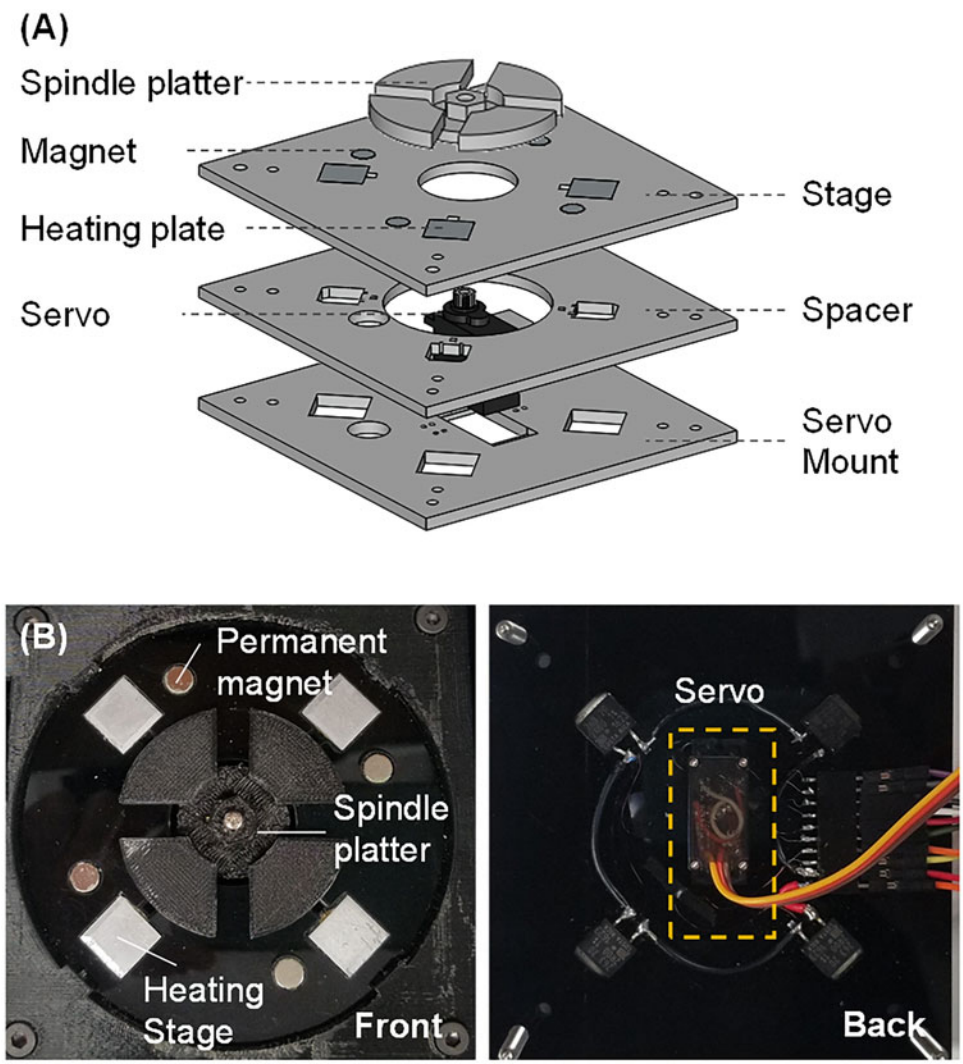

Fig. 11 Photo image and schematics of the integrated electromechanical subsystems. (**a**) Exploded view of the amounting layers. Permanent magnets and aluminum heating plates were placed on the stage layer. The level of stage layer was adjusted by a spacer to make the servo shaft exposed to the outside. (**b**) Assembled view. Spindle platter was screw-tightened on the servo motor shaft

3.4 Electro-mechanical Subsystem

1. Figure 11 shows the integrated electromechanical subsystem and components. The three laser-machined PMMA layers held the four permanent magnets, thermal modules, and servo motor for a streamlined sample process (Fig. 11a, *see* **Note 1**). Each layer was aligned with M4 screws and permanently fixed with an acrylic solvent. The servo was fixed on the servo mount layer using screws. Magnets and heating plates were tightly fit to the patterned stage layer and supported by the spacer (Fig. 11a). The permanent magnet was used to facilitate

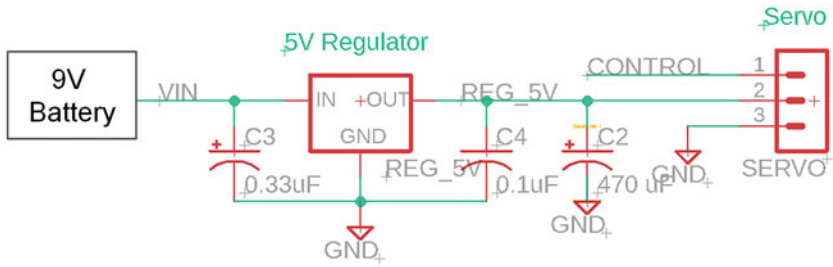

Fig. 12 Circuit diagram for an electromechanical subsystem. 9 V is regulated to 5 V using a voltage regulator. Regulated 5 V powers the servo. The control wire is connected to the PWM terminal in MCU

charge-switchable magnetic bead-based assay for the nucleic acid sample preparation (Detailed Magnetic bead-based assay is discussed in the companion Chap. 16).

2. After assembling the PMMA layers, 3D printed spindle platter was installed at the high-torque servo motor shaft to rotate the microfluidic reagent compact disc (Fig. 1b). Spindle platter was designed to avoid optical interference from the other blue LED light sources for uniform excitation among four channels (Fig. 1b).
3. Figure 12 shows the circuit diagram of the integrated electromechanical subsystem. To power the servo, we derived 5 V from 9 V battery using a voltage regulator. To prevent the power fluctuation during servo actuation, we connected a capacitor (470 μF) to the power line. The servo was controlled by the pulse width modulation (PWM) signal. For example, 1 ms, 1.5 ms, and 2 ms pulse width corresponds to the −90°, 0°, and +90° turns, respectively. Therefore, specific servo shaft position and direction of the rotation can be programmed via the PWM command in Arduino IDE.
4. The spindle platter structure holds the microfluidic reagent compact disc (Fig. 1b); thus, the disc rotates along with the servo. The magnet underneath of the disc interacts with magnetic beads inside of the reagent disc. By the disc rotating against the stationary magnet, magnetic beads can be actuated into a different location in the reagent disc (Please, refer to the companion Chap. 16).

3.5 Data/Interfacing Subsystems

1. The fluorescence signal was transferred to the internal MCU memory through I^2C communication at a constant interval (~5 s). The optical data was displayed on the LCD touchscreen or smartphone (via Bluetooth) in real-time. The LCD touchscreen breakout supports the X–Y coordinate system. Therefore, each data point can be plotted at the specified position on the screen. We assign time progression for X-coordinate and optical data for Y-coordinate.

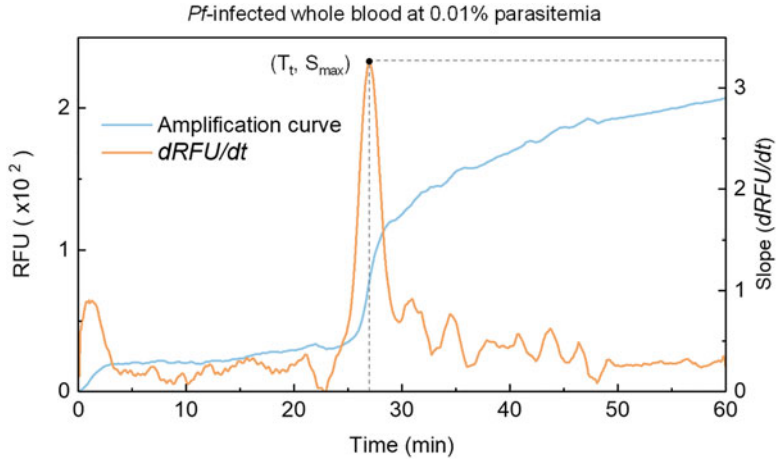

Fig. 13 Determination of the threshold time (T_t). A real-time amplification curve (blue) and the corresponding differential profile (d*RFU*/d*t*, orange). The threshold time (T_t) was determined at the maximum slope of RFU (T_t threshold time, t time, S_{max} maximum value of the slope). (Reproduced from Biosensors and Bioelectronics 2018 with permission from Elsevier [40])

2. A built-in moving average algorithm smoothed the optical signal with background noise removed. More specifically, the arithmetic mean of a given set of data (data span = 10) was taken every moving window. Open-source moving average library for Arduino IDE is available online (http://arduino.cc/playground/Main/RunningAverage).
3. The threshold time (T_t) was obtained when the slope of RFU (d*RFU*/d*t*) reached the peak (Fig. 13).
4. Collected data is saved in the micro SD card in .txt format for export.

3.6 Arduino Microcontroller Unit (MCU) Interface

1. The microcontroller board includes a microprocessor (ATmega2560), flash memory (256 kB), 16 analog inputs, 54 digital inputs/outputs, 4 serial ports, and USB connection. Arduino board can be powered by an external power source (9 V battery) using the Vin pin. 9 V input voltage is regulated down to 5 V and 3.3 V by the internal voltage regulator. ATmega2560 support two-wire serial interface (I^2C) and serial peripheral interface (SPI) for communicating with peripheral devices such as color sensor, LCD touchscreen, Bluetooth, and SD card module.
2. We stacked the customized PCB board (Fig. 4a) on top of the commercial Arduino board to reduce the wiring.
3. The control sequence for all integrated electronic devices was combined into a single program using Arduino IDE and uploaded to the MCU. Therefore, no computer connection is required to operate the analyzer.

3.7 Enclosures and System Integration

1. All enclosures (body and lid) were 3D printed using ABS material.
2. The lid enclosure was patterned to hold the LCD touch screen and four optical sensors (Fig. 1a). The bottom cover of the lid enclosure has holes to couple optical fibers for collecting green emission light.
3. Multiple laser-patterned PMMA layers were stacked together to hold aluminum heating plates, magnets, and servo (Fig. 11b). On top of the PMMA layers, we placed a 3D printed optical fiber holder to align the excitation light facing the reaction chamber (Fig. 8b).
4. Afterward, all overlaid layers were secured into the body enclosure using M4 screws.
5. Control PCB and 3D printed fiber coupler with four blue LEDs were secured on the bottom cover of the enclosure (Fig. 14).
6. All necessary electronic wires and optical fibers were connected (Fig. 14), then the bottom cover was assembled to the body enclosure.
7. The 3D printed spindle platter was assembled at the servo shaft (*see* **Note 1**).
8. Finally, body and lid enclosures were joined by the hinges.

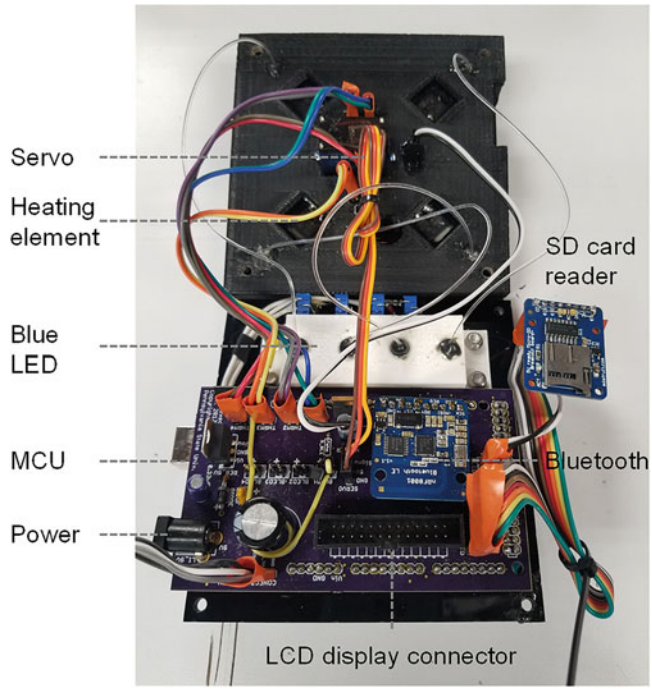

Fig. 14 Assembled analyzer without enclosure. The LCD touchscreen is connected through ribbon cables (LCD is located in the lid)

3.8 Cost Analysis

1. The prototype analyzer presented in this work could be built for a total amount of ~$245.35 (Table 2 for cost breakdown).

4 Notes

1. To minimize the optical power loss (e.g., insertion and return loss), the end surface of the fiber was first polished with 2000 grit polishing paper, then further smoothed with a 3 μm polishing film.
2. Gain and analog-to-digital converter (ADC) integration time are important photodiode parameters for the optimal fluorescence readings. While higher gain and longer integration time can amplify the optical signal and increase the sensitivity of the photodiode, the reading can exceed the dynamic range and be saturated. On the other hand, the photodiode is not enough to distinguish weak green emission light from background noise with lower gain and shorter ADC integration time. For example, the dynamic range of photocounts at 700 ms integration time is 0 to 65,535. The light intensity beyond this range will not be resolved. We experimentally confirmed that photocounts from maximum fluorescence dye concentration did not exceed the dynamic range with the selected gain (60×) and integration time (700 ms) setting (*see* a subset of Fig. 10a).
3. We used a potentiometer, which can physically adjust the resistor values by turning the knob. However, the programable approach using a Pulse Width Modulation (PWM) method can be an alternative for simply excitation LED light intensity adjustment.
4. Magnetic beads were actuated by rotating the reagent compact disc against a stationary permanent magnet. Since the magnetic force is inversely proportional to the distance squared, a small gap between the disc bottom and the magnet top can cause the failure of magnetic bead actuation. For the reliable magnetic actuation, a flat permanent magnet holding layer is desired.
5. A 90-degree rotational turn of a servo is sufficient to cover the entire testing unit on microfluidic reagent disc. We set the servo angle (90°) as a reference position to maximize the range of rotational motion. During the spindle platter assembly, we placed the reaction chamber in the microfluidic disc to vertically align with the permanent magnet position.

Acknowledgments

This work was supported by grants National Science Foundation under Grant No. 1710831, 1912410, and 1902503. We express

our gratitude to Dr. Liwang Cui, Dr. Jun Miao, and Xiaolian Li for providing cultured malaria samples. W.G. acknowledges the support from Penn State Startup Fund.

References

1. Vashist SK (2017) Point-of-care diagnostics: recent advances and trends. Biosensors (Basel) 7(4):62
2. Vashist SK, Luppa PB, Yeo LY et al (2015) Emerging Technologies for Next-Generation Point-of-Care Testing. Trends Biotechnol 33 (11):692–705
3. Mauk M, Song J, Bau HH et al (2017) Miniaturized devices for point of care molecular detection of HIV. Lab Chip 17(3):382–394
4. Laksanasopin T, Guo TW, Nayak S et al (2015) A smartphone dongle for diagnosis of infectious diseases at the point of care. Sci Transl Med 7(273):1–11
5. Chiu DT, deMello AJ, Di Carlo D et al (2017) Small but perfectly formed? Successes, challenges, and opportunities for microfluidics in the chemical and biological sciences. Chem 2 (2):201–223
6. Chen H, Liu K, Li Z et al (2019) Point of care testing for infectious diseases. Clin Chim Acta 493:138–147
7. Wu L, van den Hoogen LL, Slater H et al (2015) Comparison of diagnostics for the detection of asymptomatic *Plasmodium falciparum* infections to inform control and elimination strategies. Nature 528(7580):S86–S93
8. Hopkins H, Gonzalez IJ, Polley SD et al (2013) Highly sensitive detection of malaria Parasitemia in a malaria-endemic setting: performance of a new loop-mediated isothermal amplification kit in a remote Clinic in Uganda. J Infect Dis 208(4):645–652
9. Vallejo AF, Martinez NL, Gonzalez IJ et al (2015) Evaluation of the loop mediated isothermal DNA amplification (LAMP) kit for malaria diagnosis in *P. vivax* endemic settings of Colombia. PLoS Negl Trop Dis 9(1):e3453
10. Modak SS, Barber CA, Geva E et al (2016) Rapid point-of-care isothermal amplification assay for the detection of malaria without nucleic acid purification. Infect Dis 9:1–9
11. Aydin-Schmidt B, Xu WP, Gonzalez IJ et al (2014) Loop mediated isothermal amplification (LAMP) accurately detects malaria DNA from filter paper blood samples of low density Parasitaemias. PLoS One 9(8):e103905
12. Morris U, Khamis M, Aydin-Schmidt B et al (2015) Field deployment of loop-mediated isothermal amplification for centralized mass-screening of asymptomatic malaria in Zanzibar: a pre-elimination setting. Malar J 14:1–6
13. Han ET, Watanabe R, Sattabongkot J et al (2007) Detection of four plasmodium species by genus- and species-specific loop-mediated isothermal amplification for clinical diagnosis. J Clin Microbiol 45(8):2521–2528
14. Polley SD, Mori Y, Watson J et al (2010) Mitochondrial DNA targets increase sensitivity of malaria detection using loop-mediated isothermal amplification. J Clin Microbiol 48 (8):2866–2871
15. Safavieh M, Kanakasabapathy MK, Tarlan F et al (2016) Emerging loop-mediated isothermal amplification-based microchip and microdevice Technologies for Nucleic Acid Detection. ACS Biomater Sci Eng 2 (3):278–294
16. Tomita N, Mori Y, Kanda H et al (2008) Loop-mediated isothermal amplification (LAMP) of gene sequences and simple visual detection of products. Nat Protoc 3(5):877–882
17. Goto M, Honda E, Ogura A et al (2009) Colorimetric detection of loop-mediated isothermal amplification reaction by using hydroxy naphthol blue. BioTechniques 46(3):167–172
18. Notomi T, Mori Y, Tomita N et al (2015) Loop-mediated isothermal amplification (LAMP): principle, features, and future prospects. J Microbiol 53(1):1–5
19. Kim J, Johnson M, Hill P et al (2009) Microfluidic sample preparation: cell lysis and nucleic acid purification. Integr Biol 1(10):574–586
20. Myers FB, Henrikson RH, Bone J et al (2013) A handheld point-of-care genomic diagnostic system. PLoS One 8(8):e70266
21. Liao SC, Peng J, Mauk MG et al (2016) Smart cup: a minimally-instrumented, smartphone-based point-of-care molecular diagnostic device. Sensor Actuat B Chem 229:232–238
22. Liu CC, Mauk MG, Hart R et al (2012) A low-cost microfluidic Chip for rapid genotyping of malaria-transmitting mosquitoes. PLoS One 7(8):e42222
23. Choi S (2016) Powering point-of-care diagnostic devices. Biotechnol Adv 34(3):321–330
24. Abel G (2015) Current status and future prospects of point-of-care testing around the globe. Expert Rev Mol Diagn 15(7):853–855

25. Jung WE, Han J, Choi JW et al (2015) Point-of-care testing (POCT) diagnostic systems using microfluidic lab-on-a-chip technologies. Microelectron Eng 132:46–57
26. Singleton J, Osborn JL, Lillis L et al (2014) Electricity-free amplification and detection for molecular point-of-care diagnosis of HIV-1. PLoS One 9(11):e113693
27. Curtis KA, Rudolph DL, Morrison D et al (2016) Single-use, electricity-free amplification device for detection of HIV-1. J Virol Methods 237:132–137
28. Stedtfeld RD, Tourlousse DM, Seyrig G et al (2012) Gene-Z: a device for point of care genetic testing using a smartphone. Lab Chip 12(8):1454–1462
29. Gorkin R, Park J, Siegrist J et al (2010) Centrifugal microfluidics for biomedical applications. Lab Chip 10(14):1758–1773
30. Kim TH, Park J, Kim CJ et al (2014) Fully integrated lab-on-a-disc for nucleic acid analysis of foodborne pathogens. Anal Chem 86 (8):3841–3848
31. Dineva MA, MahiLum-Tapay L, Lee H (2007) Sample preparation: a challenge in the development of point-of-care nucleic acid-based assays for resource-limited settings. Analyst 132 (12):1193–1199
32. Kolluri N, Klapperich CM, Cabodi M (2018) Towards lab-on-a-chip diagnostics for malaria elimination. Lab Chip 18:75–94
33. Lucchi NW, Gaye M, Diallo MA et al (2016) Evaluation of the Illumigene malaria LAMP: a robust molecular diagnostic tool for malaria parasites. Sci Rep 6:36808. https://doi.org/10.1038/srep36808
34. Sema M, Alemu A, Bayih AG et al (2015) Evaluation of non-instrumented nucleic acid amplification by loop-mediated isothermal amplification (NINA-LAMP) for the diagnosis of malaria in Northwest Ethiopia. Malar J 14. https://doi.org/10.1186/s12936-12015-10559-12939
35. Jani IV, Meggi B, Vubil A et al (2016) Evaluation of the whole-blood Alere Q NAT point-of-care RNA assay for HIV-1 viral load monitoring in a primary health care setting in Mozambique. J Clin Microbiol 54 (8):2104–2108
36. Hsiao NY, Dunning L, Kroon M et al (2016) Laboratory evaluation of the Alere q point-of-care system for early infant HIV diagnosis. PLoS One 11(3):e0152672
37. Nolte FS, Gauld L, Barrett SB (2016) Direct comparison of Alere i and cobas Liat influenza a and B tests for rapid detection of influenza virus infection. J Clin Microbiol 54 (11):2763–2766
38. Gous N, Scott L, Berrie L et al (2016) Options to expand HIV viral load testing in South Africa: evaluation of the GeneXpert (R) HIV-1 viral load assay. PLoS One 11(12): e0168244
39. Dormond L, Jaton K, de Valliere S et al (2015) Malaria real-time PCR: correlation with clinical presentation. New Microbes New Infect 5:10–12
40. Choi G, Prince T, Miao J et al (2018) Sample-to-answer palm-sized nucleic acid testing device towards low-cost malaria mass screening. Biosens Bioelectron 115:83–90
41. Choi G, Song D, Shrestha S et al (2016) A field-deployable mobile molecular diagnostic system for malaria at the point of need. Lab Chip 16(22):4341–4349
42. Xu G, Nolder D, Reboud J et al (2016) Paper-origami-based multiplexed malaria diagnostics from whole blood. Angew Chem 55 (49):15250–15253
43. Britton S, Cheng Q, Sutherland CJ et al (2015) A simple, high-throughput, colourimetric, field applicable loop-mediated isothermal amplification (HtLAMP) assay for malaria elimination. Malar J 14:335
44. Nair CB, Manjula J, Subramani PA et al (2016) Differential diagnosis of malaria on Truelab Uno(R), a portable, real-time, MicroPCR device for point-of-care applications. PLoS One 11(1):e0146961
45. Taylor BJ, Howell A, Martin KA et al (2014) A lab-on-chip for malaria diagnosis and surveillance. Malar J 13:179. https://doi.org/10.1186/1475-2875-1113-1179
46. Liu Q, Nam J, Kim S et al (2016) Two-stage sample-to-answer system based on nucleic acid amplification approach for detection of malaria parasites. Biosens Bioelectron 82:1–8
47. Shin Y, Lim SY, Lee TY et al (2015) Dimethyl adipimidate/thin film sample processing (DTS); a simple, low-cost, and versatile nucleic acid extraction assay for downstream analysis. Sci Rep 5:14127. https://doi.org/10.1038/Srep14127
48. Li Y, Kumar N, Gopalakrishnan A et al (2013) Detection and species identification of malaria parasites by isothermal, tHDA amplification directly from human blood without sample preparation. J Mol Diagn 15(5):634–641